IEEE Photonics Journal
An IEEE Photonics Society Publication

Open Access

High Density Multi-Channel Passively Aligned Optical Probe for Testing of Photonic Integrated Circuits

Volume 13, Number 1, February 2021

Xaveer Leijtens, ***Senior Member, IEEE***
Rui Santos
Kevin Williams, ***Member, IEEE***

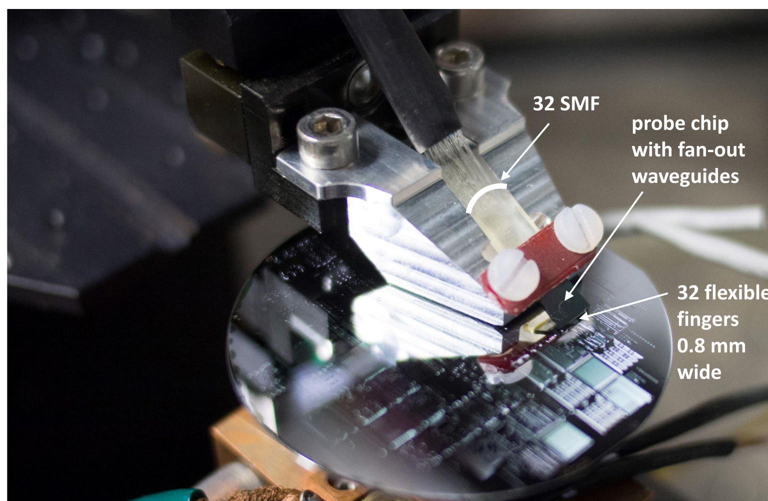

DOI: 10.1109/JPHOT.2020.3045346

IEEE photonics SOCIETY
IEEE

High Density Multi-Channel Passively Aligned Optical Probe for Testing of Photonic Integrated Circuits

Xaveer Leijtens,[1] *Senior Member, IEEE*, Rui Santos,[2] and Kevin Williams,[1] *Member, IEEE*

[1]Institute for Photonic Integration, Eindhoven University of Technology, 5600 MB, Eindhoven, Netherlands
[2]PhotonIP BV, 5614 BC, Eindhoven, Netherlands

DOI:10.1109/JPHOT.2020.3045346
This work is licensed under a Creative Commons Attribution 4.0 License. For more information, see https://creativecommons.org/licenses/by/4.0/

Manuscript received October 13, 2020; accepted December 11, 2020. Date of publication December 15, 2020; date of current version January 7, 2021. This work was supported by the Dutch Research Council (NWO), Project ProCon 11369. Corresponding author: Xaveer Leijtens. (e-mail: x.j.m.leijtens@tue.nl).

Abstract: In this work we report the results of high density multi-channel optical multiprobes with pitches of 25 μm and 50 μm that provide edge-coupling used for on-wafer parallel testing of photonic integrated circuits. The probes are fabricated in an oxynitride platform and test demonstrations were carried out of edge-coupled indium-phosphide based photonic integrated circuits (PICs). Thirty-two optical parallel connections are simultaneously, passively aligned between the probe and the PIC by means of integrated guiding channels. The initial placement tolerance is more than 4 μm to give a passive alignment with an optical power variation of less than 1 dB. Multi-port loop-back optical power measurements are reported and the wavelength-dependent net modal gain of integrated semiconductor optical amplifiers was measured to further validate the concept.

Index Terms: Photonic integrated circuits, optical probing, fiber-chip coupling.

1. Introduction

The integration density of photonic integrated circuits is rapidly increasing, following an exponential trend similar to what is called Moore's law in micro-electronics [1]. This is mainly driven by a wider range of applications such as data communication [2] and sensing [3] that use photonic integrated circuits (PICs) as their core technology. The main photonic integration platforms that are used today are the monolithically integrated InP-based and heterogeneous or hybrid Si-based technology platforms. The increase of the component density and complexity has a direct impact on the application spectrum and on the overall performance of the PICs. To fully enable this growth, multi-port optical interfaces (I/Os) and novel testing concepts are called for. Currently, no practical methods are available that allow multiport precision on-wafer optoelectronic testing of each photonic device or circuit because there is no good way to provide for the optical connections. For multiport PIC packaging, a number of solutions have been proposed [4]–[6].

Testing is a recurrent and complex problem in the manufacturing process of PICs. The lack of solutions that allow for tolerant alignment with multiple ports for parallel testing between the external instrumentation and the photonic IC makes testing a time consuming and non-scalable operation. For alignment in general, both active and passive alignment schemes are in use. Active

alignment requires first a passive alignment step, based on a visual system or on pre-calibration, that brings the two optical device elements within a range where "first light" is detected [7], [8]. After that, a feedback loop between the positioning stages and an optical power meter is setup which is used to maximize the optical power coupling. This alignment procedure is generally slow, complex (in particular when aligning more than one optical interface simultaneously) and it requires high-precision movement actuators ($<$50 nm). Furthermore, two main optical coupling approaches exist: edge-coupling and coupling via surface gratings. Edge-coupled devices have the advantage of broadband optical response, but access to the waveguide is not available until after the chips have been singulated from the wafer. Since the mode size of a standard single-mode fiber (SMF) and the waveguide may differ significantly (typically a factor 5–20), either mode-size converters are required or sub-micron alignment may be needed, or a combination of both. Grating couplers couple out-of-plane to a near-vertical direction and are manufacturable in thin membrane-type high-contrast waveguides, typically in Si-based integration technologies. They are accessible before chip singulation and thus allow on-wafer probing, but they are wavelength and polarization dependent and induce reflections [9]. These structures are typically designed to have a mode-field-diameter (MFD) of around 10 μm, matching that of an SMF, which allows for a more relaxed alignment (1-dB penalty within $\pm$2.5 μm offset), but with a trade-off on angular alignment [10], [11].

Multi-port optical testing probe-heads have been developed using MEMS technology [12], but this technology adds complexity and extra processing to fabricate extra mechanical structures for the alignment between the probe head and the optical interfaces. Single optical probe systems using 6-axis alignment translations stages [13] have been developed in combination with standard electrical probing systems [14], but these systems do not allow multi-port parallel testing and they require active alignment between the optical probe and the PIC.

Although more advanced solutions using multiple port optical interposers for vertical coupling combined with electrical probing have been reported [15], these still rely on grating couplers, require active alignment and are not suited for edge emitting photonic integration platforms. For multi-port testing and on-wafer probing, probe heads have been reported using technology with a total internal reflection element that redirects the light collected from a trench in front of on-wafer waveguides [16], [17]. These approaches tackle the multiple port issue and the possibility to run optical tests before separation of the individual PICs but the alignment between the probe and the PIC waveguides is challenging because sub-micron active alignment on at least three axes is required to achieve optimum optical power coupling.

InP-based devices may make use of their capability to generate and detect light. This characteristic could be an advantage over other photonics platforms because it allows for the design of test structures with integrated sources and detectors and thus enables all-electrical testing for many of the process control modules [18]. Having such test structures improves the overall testability but some tests, for example absolute wavelength compliance, can only be performed at the end of the fabrication process. To solve this problem, other approaches focused on the development of structures to access the light from the waveguides prior to cleaving the wafer into single devices or bars of devices. Fundamental work developed by Vettiger *et al.* [19] showed the potential of using etched facets for testing light-generating devices. Slanted mirrors in front of the etched facet have also been demonstrated to allow for vertical collection of the light propagating out of the waveguide [20]. However, extra processing steps are required and no method has been presented for passive alignment.

In this paper we present a novel high-density multi-port optical probe, fabricated in oxynitride technology, capable of on-wafer probing for optical testing and characterization of photonic ICs. The alignment process between the optical probe and the PIC is passive and optimum optical alignment is achieved with an initial micron-accuracy probe placement. A detailed description of the SiN optical probe, of the InP PIC structures required for the self-alignment and of the passive alignment process is presented in Section 2. In Section 3 we demonstrate a high port-density with a pitch of 25 μm, interfaced to 32 SMF fibers, and describe the calibration method of the probe. We experimentally analyze the passive alignment tolerance between the interface structure and an InP-based PIC and perform a detailed study of the chip-to-fiber coupling efficiency. Finally, we

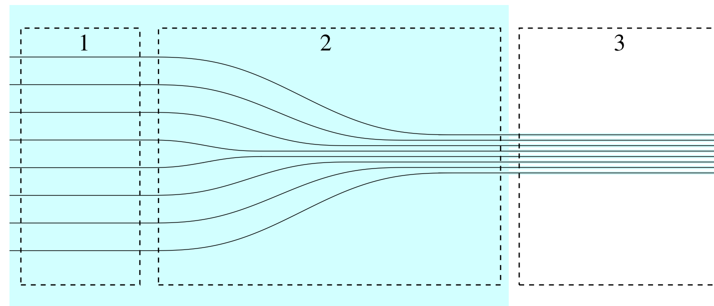

Fig. 1. Simplified mask layout of an eight-port multiprobe. Three regions are indicated: region 1 is where the fiber-array unit is connected. The pitch of the waveguides is typically 127 μm. Region 2 is the fan-in region where the waveguide pitch is reduced to 25 or 50 μm. Region 3 is where the waveguides are separated and the substrate below the waveguides is removed to create the flexible fingers.

demonstrate on-wafer optoelectronic testing by measuring the small signal modal gain of integrated semiconductor optical amplifiers.

2. Concept Description

In this section, we describe the high density multi-port optical coupler that will interface between a photonic integrated circuit (PIC) and an array of SMF fibers and the alignment procedure.

2.1 Optical Probe Design and Fabrication

The multi-port optical coupler is fabricated in the TriPleX oxynitride platform [21]. A schematic of the optical probe is shown in Fig. 1. The structure is characterized by 3 sections that each perform a specific function:

1) Fiber array unit (FAU) interface: in this region, the waveguide pitch and the mode size are matched between the fiber array and the TriPleX waveguide structures.
2) On-chip routing: in this region, the optical mode confinement is higher to allow for smaller bend-radius. The simplest function of this region is to adapt the pitch and mode size between fiber array, the on-chip waveguide array and the mode size of the InP waveguide. If desired, more complex optical functions that exploit the unique properties of the oxynitride waveguide structure can be added.
3) Flexible waveguide beams (see Fig. 2 for details): in this area the substrate is removed underneath the waveguides and thin and long free-standing waveguide beams, or fingers, are formed. Because of their dimensions, the fingers are flexible. The cladding and the width of the TriPleX fingers are designed to match the etched structure that is defined in the InP PIC. The optical waveguides in the fingers are laterally centered. The waveguide in the finger is single mode and the mode size is matching that of the fundamental mode of the InP waveguide. The 1/e ^{2} mode diameter of both modal fields is approximately 2×1 μm (lateral $\times$ transverse).

Several devices have been fabricated with 4, 8 and 32 flexible waveguides in the same probe and 2 different pitches, 25 μm and 50 μm. This design was tailored for specific InP platforms. When used for other planar waveguide technologies, such as the silicon photonics platforms, the dimensions of the probe will need adaptation to the specific dimensions of that platform.

2.2 InP Counterpart

On the InP PIC we designed mechanical guiding structures that ensure the passive alignment of the fingers in funnel-shaped guides, ending at the etched facets of the PIC waveguides. A scanning electron microscope of such structures is presented in Fig. 3. The waveguide termination is defined

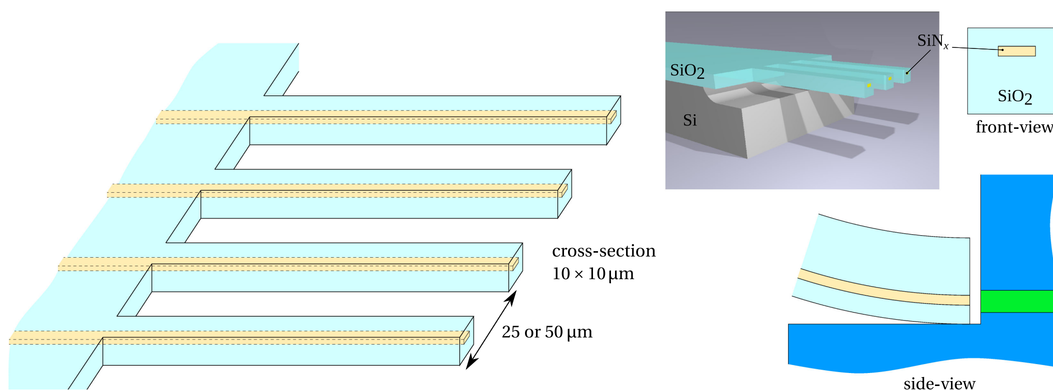

Fig. 2. Schematic view of the flexible fingers in region 3 of Fig. 1. Typical length of the fingers is 500–750 μm. The right figures show the front view at the top and a side view below, with a schematic of the coupling to an InP waveguide (center line cross section). Note that when coupling, the finger waveguides are upside-down.

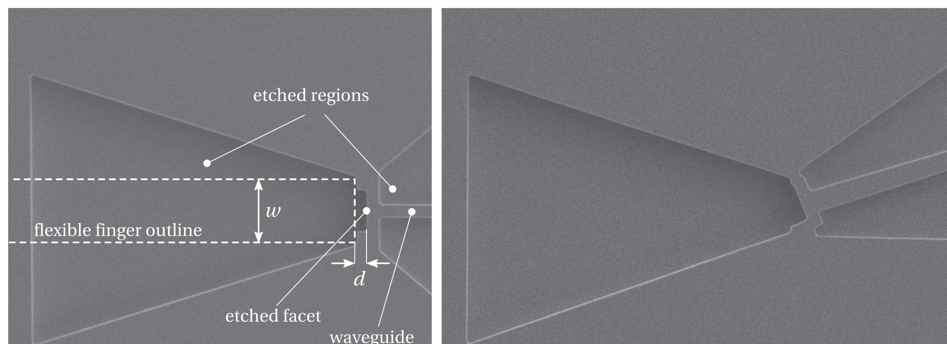

Fig. 3. Scanning electron microscope images of waveguides with etched facets and triangular alignment area. (left) The image shows an annotated straight-facet waveguide. The width w of the finger matches the width of the end of the funnel and d is the distance between the end of the finger and the etched facet. (right) This shows an image of an angled facet waveguide interface. The fingers connecting to either angled or straight waveguides are identical and at an identical position with respect to the alignment area.

by etching a facet which is less than 5° from the vertical direction. This allows the optical I/Os to be positioned anywhere on chip or wafer, without being restricted to the edge of the chip. The etch depth of these structures was chosen to be one of the standard etch levels available in the TU/e-SMART Photonics and OCLARO InP platforms [22], [23], thus not requiring any process adaptations for using the probes. The etching process provided by these platforms allows for high quality facets [20].

Two different configurations of etched facets were fabricated, one with straight etched facets (Fig. 3, left) where the facet is defined normal to the propagation of the light in the waveguide and an angled-facet where the facet is defined with an angle of 7° with respect to the normal of the propagation direction (Fig. 3, right), allowing for a low-reflection interface. Both designs are compatible with the optical probes described in the previous section, so no re-design is needed in the probe side to accommodate for straight or angled optical couplings.

The design of the etched facet structure includes a funnel-shaped self-alignment structure in the lateral direction and a mechanical displacement stopper in the longitudinal direction, see Fig. 3. These are designed to match the width $w = 10$ μm of the flexible finger and keep it at a fixed distance, thus creating an air gap of $d = 2.5$ μm. The alignment in the vertical (out-of-plane)

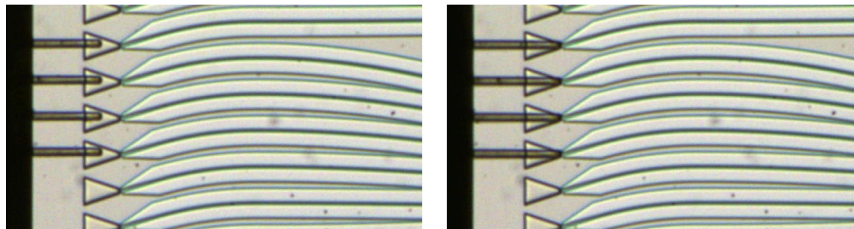

Fig. 4. Photograph of 4-finger array with 50 μm pitch on landing zone (left) and aligned to four waveguides with etched angled facets (right).

direction is defined by the etch depth of the InP and the thickness of the top cladding of the flexible suspended beams. If needed, these structures can be used as permanent interfaces to the probes for packaging purposes. However, in case a standard approach with optical fibers is needed, the funnel structures, when properly placed, can be cleaved off accurately [24], and the etched facet can be used for coupling to a (lensed) fiber array, taking into account the limitations on pitch.

2.3 Passive Alignment

The solution presented here requires only passive alignment to have maximum optical power coupling. In our configuration the InP PIC was mounted in a single-plane rotation stage and the first step is to place the probe's flexible waveguides on top of the InP self-alignment area followed by a coarse rotation alignment Fig. 4 (left), without optical signal monitoring. Then, the probe is moved down towards the InP until there is contact (probes landed on the InP) between the chips. The final step is to move the probe in the focus direction to bring the flexible waveguides to the stop position in front of etched facet, see Fig. 4 (right). None of these alignment steps require sub-micron position-stage control.

3. Experimental Demonstration

The experimental demonstration of the multi-probe is described in this section. First, we report on the testing capabilities of a 32-port optical probe and its calibration procedure. Next, we determine the passive alignment tolerances and we analyze the overall coupling loss. Finally, to validate the procedure, we present measurements of the gain spectrum of semiconductor optical amplifiers using the optical probe as an out-coupler.

The probes and InP counterpart used in the experiments have not been provided with an anti-reflection coating. To obtain proper results and to not be affected by power fluctuations due to possible interference effects, we have used a broadband source. Because the modal fields on both sides of the interface are matched, we expect only a very weak wavelength and polarization dependence. This has not been experimentally verified in this work.

3.1 High Density Multi-Port Testing

To carry out the experimental characterization of the optical probe devices, a probe holder has been designed for mounting and handling. It can hold any of the fabricated optical probes, and it is compatible with standard 1-μm-resolution 3D manual translation stages that are typically used in electrical probe test systems. This is shown in Fig. 5 where a 32-port optical I/O probe is placed in the holder. In this picture we used a 2” InP wafer which contains several optical circuits, which were designed and fabricated to be compatible with this optical probe testing.

To demonstrate the multi-port testing capabilities, a calibration of the relative transmission for each of the optical channels was first carried out. The calibration was obtained with two different multiprobes, one input and one output, in transmission configuration through an InP waveguide.

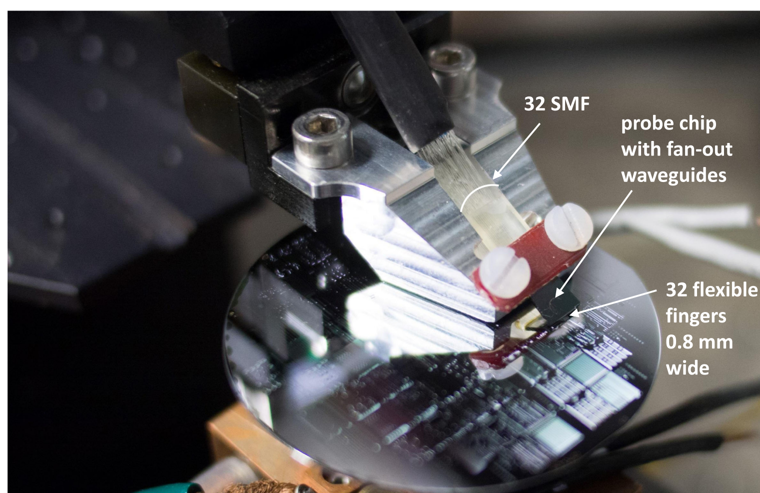

Fig. 5. On-wafer probing of a 2” wafer with 32 simultaneous optical connections. The multiprobe chip measures 5 × 5 mm^2 and contains the fan-out waveguides connecting a 32-SMF fiber array with 127-μm pitch to a 32-finger array which has 25-μm pitch and a total width of 0.8 mm.

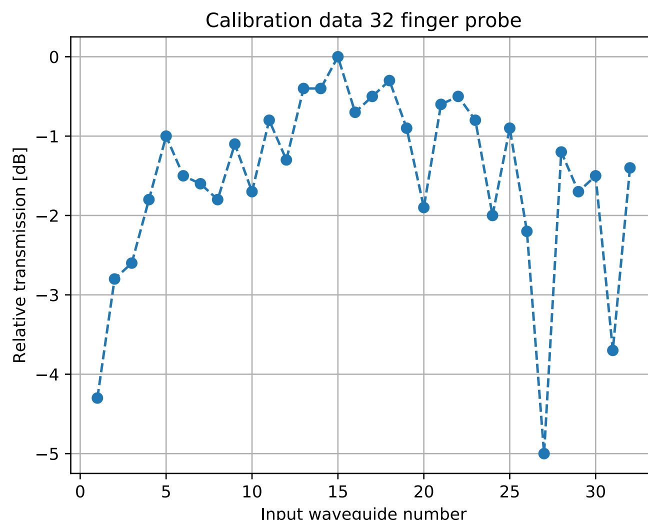

Fig. 6. Calibration curve of a 32-channel optical multiprobe. The transmission power is normalized to the maximum measured value. The variation is mainly caused by the difference in coupling efficiency from the fiber array to the multiprobe chip.

We fixed one of the optical channels of the second multiprobe on one end of an InP waveguide and aligned to the other end, in sequence, each one of the fingers of the 32-port probe that was under calibration and measured the optical power. A C+L broadband light source (Alxenses OLS15CL) and a HP 81531 A power meter were used to carry out this experiment.

The results are presented in Fig. 6 where we can observe that the inner channels show a higher relative transmission than the outer ones. A maximum difference of 5 dB was measured between channels 15 and 27. The systematic variation in the optical transmission between each channel of the optical probe is attributed to misalignment in the attachment process between the FAU and the multiprobe chip. Another cause for variation could be imperfections in the probe waveguides. The data presented in Fig. 6 is used to calibrate the relative transmission of each of the fingers in the 32-finger probe.

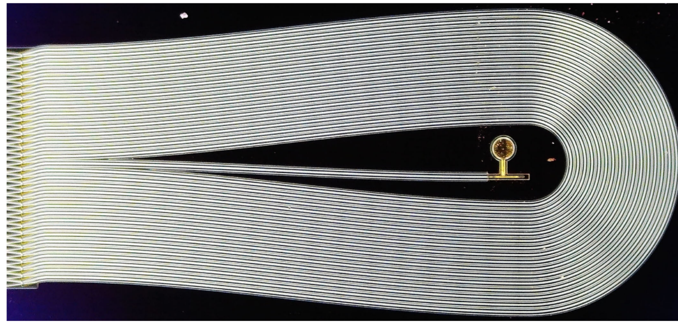

Fig. 7. Waveguide layout of 32 loop-back InP waveguides. The center waveguide is connected to an on-chip pin photo-diode, which is not used in this work.

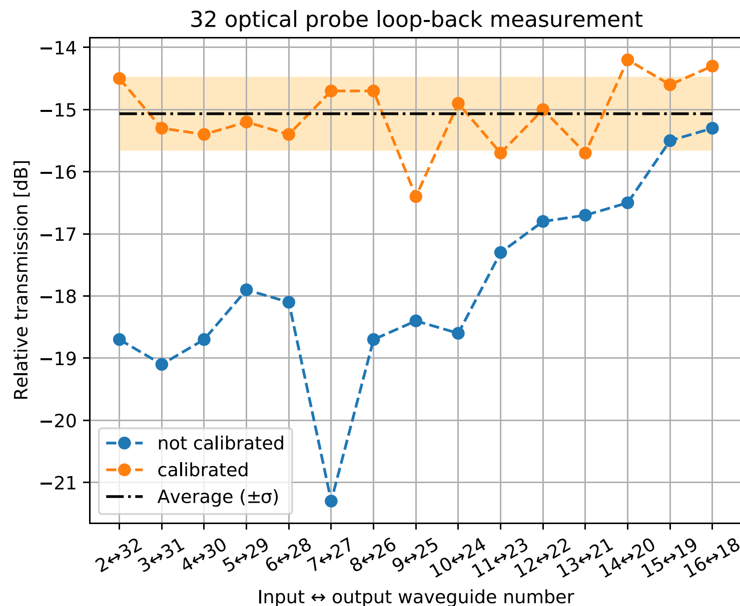

Fig. 8. Transmission through finger-pairs connected by loop-back InP waveguides. The data in the upper curve has been calibrated with the measurements shown in Fig. 6.

After the calibration, we tested this probe in a 32 loop-back waveguide test structure fabricated in InP (Fig. 7). This structure comprises 32 loop-back waveguides, with an on-chip pin photo-diode connected to the center waveguide in position 17, which was included in the design for developments not related to this work. In this way, loop-back connections were made between finger pairs 2–32, 3–31 ,..., 15–19, 16–18. Fingers 1 and 17 are not used in this experiment, so 15 pairs (30 connections) were tested. The measured transmission through the loop-back InP waveguides is shown in Fig. 8.

The data, before correction, shows a positive slope in the optical power which is due to the transmission difference between the inner and outer fingers. As expected, there is a dip in transmitted power between channels 7–27 because channel 27 showed the minimum measured optical power in the calibration (Fig. 6). After correcting the measured loop-back transmission data for the relative difference of each pair we expect the same value for each pair, since the InP waveguides are almost equal in length. Indeed, all 15 channel pairs show only a standard deviation of $\pm$0.6 dB from the average power level, as indicted in the same figure. The result validates the use of the probe for high-density optical testing and validates the calibration method since the variation in

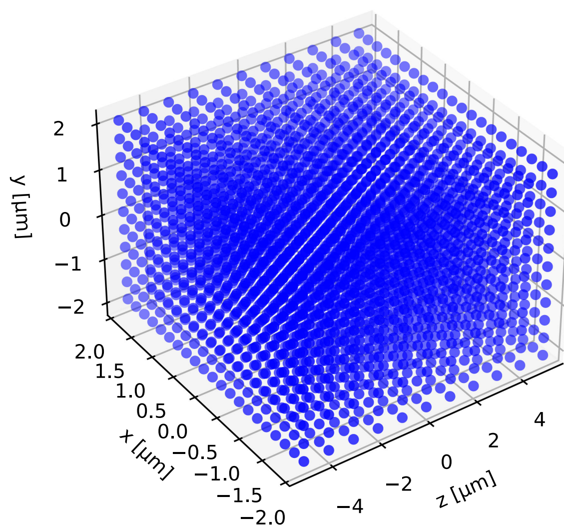

Fig. 9. Placement locations of the 8-finger multiprobe. Each location is randomly visited once during the full measurement sequence.

transmission loss between different waveguides in the InP PIC due to a different path length is small. The absolute loss values in these measurements are accounted for in Section 3.3.

3.2 Determination of the Passive Alignment Tolerance

To determine the tolerance and passive alignment robustness in the optical interface we carry out a large sequence of optical transmission measurements for different positions of the optical probe relative to the InP. This way we can relate and analyze the variation of the optical power for each position of the probe and determine the alignment tolerance. Each measurement starts with the finger probe placed in a "park" position, where the fingers are at position $(x, y, z = 8, 55, 20)$ μm from the center of the measurement range and where they are not touching the InP PIC. The probe movement is programmed to go to a pre-defined (x, y, z) optical contact position. That movement is carried out as follows: first movement is to the x position (lateral), then to the y-position (down) and finally it moves forward to the z-position. The position of the probe is done by a computer-controlled x, y, z Newport NPXYZ100SG-D translation stage which has a closed-loop repeatability of 30 nm. This assures that the determination of the alignment tolerance of the probe is not influenced by the positioning specifications of the translation stages.

We programmed a total of $21 \times 11 \times 11 = 2541$ positions into a Python-controlled automated setup, which controls the (x, y, z) end-position of the finger probe, within a space of $(\Delta x, \Delta y, \Delta z) = (4, 4, 10)$ μm. These positions are graphically represented in Fig. 9. During the measurement sequence, the positions are each visited in a random order, which was obtained by shuffling the positions with the *shuffle* method from python's *random* module.

For this experiment we used an 8-finger optical multiprobe with a pitch of 25 μm. The InP circuit used for this experiment is a set of looped-back waveguides with etched facets at a pitch of 50 μm, fabricated by Oclaro in a multi-project wafer run [22]. The top of Fig. 10 shows the InP PIC and the probe is in park position. In the bottom figure the probe is placed on the PIC in one of the position settings from Fig. 9. Because of the difference in pitch between multiprobe and PIC waveguides, only every other finger is used and thus four of the eight fingers in the probe are connected to either end of the two inner looped-back waveguides. The other four fingers rest on top of the sample and don't play a role in the measurement. This illustrates an advantage of the coupling concept because it shows that a probe with a certain pitch may be used to test a PIC with a different optical waveguide pitch.

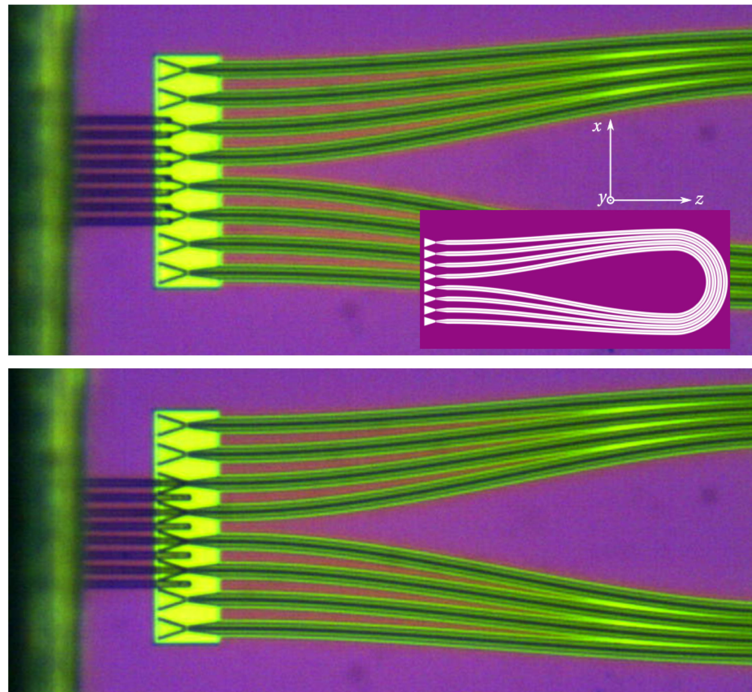

Fig. 10. Alignment with 8-finger multiprobe with 25 μm pitch to a loop-back structure used for measuring the transmission as a function of position. The upper photograph shows the fingers in “park-position,” above the chip and away from the optimum position. The inset shows the mask layout of the waveguide loops that are partly visible in the photographs. The lower photograph shows the fingers aligned to the loops. Because the loops use a 50 μm pitch, only every other finger is connected, leaving the remaining fingers on the surface of the chip, which does not impact the measurement.

The light from the broadband light source is split with a 3-dB fiber splitter and each of the two splitter outputs connects to one of the fiber inputs of the finger probe number 1 and 3. Two power meters (HP 81531 A) are connected to the fiber outputs of fingers 5 and 7. When the probe is at the specified (x, y, z) position, the power from a broadband source, transmitted through the loop-back waveguide, is recorded by the power meters, after which the finger probe moves back to the park position and the procedure is repeated until this operation is done for all positions that are depicted in Fig. 9. As each measurement sequence takes around 3 seconds, the total experiment took approximately 2.5 hours for measuring the 2541 data points. After the measurements completed, the data points were sorted again before plotting. Representative results extracted from these measurements are plotted in Fig. 11. This figure shows the normalized power transmission from the source, through the fiber splitter, through finger 1, through the loop-back waveguide and to the corresponding finger 7 in the probe which is connected to the power meter via its fiber. Similar results were obtained for the other pair of channels (3 and 5). This data is a cross section for one specific x-value. In this plot it can be seen how the power is low when the finger z-position (longitudinal) has not yet reached the waveguide facet, up to the point where the z-position is around 0 μm. Beyond this position the power remains almost constant. The point where the finger is at the designed optimum position is dependent on the vertical y-direction as well, as the fingers are touching the sample at an angle. Therefore, moving the fingers down leads to a forward (z) motion of the tip of the fingers. Once the contact with the end of the funnel is reached, there is very little dependence of the power on the y or z position of the probe holder since the extra displacement is now absorbed by the flexibility of the fingers and the tip of the finger stays in the same position. To understand the dependence of the coupling on the lateral x-position, the transmitted power at position $z = 2$ μm is plotted in Fig. 12. For comparison, relative transmission as a function of the x-displacement for a Gaussian beam with a diameter ($1/e^2$) of 10, 3 and 1 μm are added to this

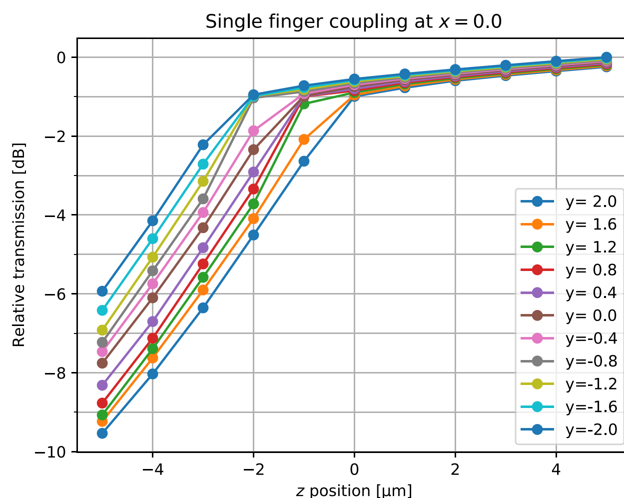

Fig. 11. Coupling loss of a single fiber-chip coupling, dependence on lateral (z) misalignment, at the center value of x.

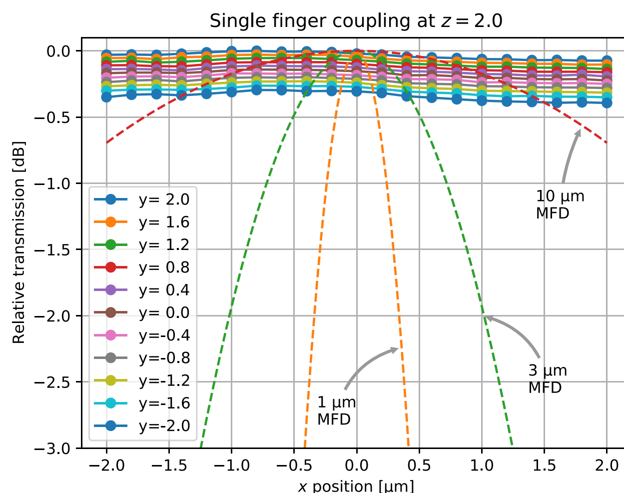

Fig. 12. Coupling transmission excess loss versus initial lateral placement, normalized to the maximum transmission. For reference, we also show the power coupling transmission between two identical Gaussian fields with 10, 3 and 1 μm mode field diameter, respectively, versus placement offset.

plot with dashed lines. These represent the equivalent Gaussian mode diameter of a standard single-mode fiber, an ultra high numerical aperture fiber and of a high-contrast waveguide. These curves are the calculated power overlaps when assuming perfect mode matching between pairs of 10, 3 and 1 μm width.

The first observation from Fig. 12 is that within 4 μm of x-displacement the coupling varies by less than 0.1 dB showing how extremely tolerant the self-alignment is in the x-direction. This result can be compared to normal mode overlap values that are indicated in the same figure for mode-field diameters of 1, 3 and 10 μm. The multiprobe compares favorably even to the overlap of two fields with 10 μm MFD, which shows a 0.7 dB excess loss for ± 2 μm placement accuracy.

Second, we notice that the self-alignment with the flexible fingers is very reproducible: each of the measured values is in a predictable position, even though the measurements are taken in a random order. Each different x-position value is on a smooth line with the previous and next points and the curves are only slightly shifted for each different y-position. This also proves that there is no damage done to the facet of the InP PIC or to the fingers themselves during the 2541

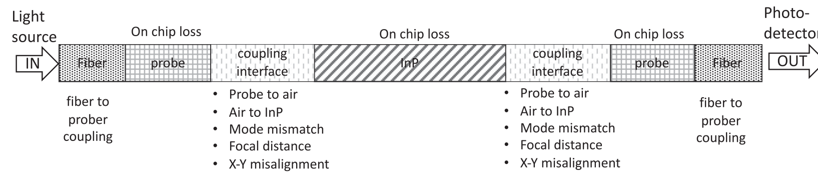

Fig. 13. Interface description and loss mechanisms at each interface between the input and the output of the probe. This is a schematic representation of a single channel measurement such as shown, for example, in Fig. 10.

TABLE 1

Summary of Estimated Loss in Each Interface and Propagation Medium for the 8-Finger Multiprobe and the InP Chip Used in the Measurement. The Last Column Lists the Expected Loss in an Optimized Version

Cause \ Loss	Fabricated probe [dB]	Optimized probe [dB]
Fiber to probe	1.5	0.5
Probe loss	0.5	0.2
Probe to air (n=1.57 to n=1)	0.2	0.0
Air to InP (n=1 to n=3.36)	1.9	0.0
Probe to InP (mode mismatch)	1.7	$<$0.3
Probe to InP (focal distance)	3.0	$<$0.5
Probe to InP (x-y mismatch)	3.5	$<$0.1
InP on-chip	1.3	1.3
Total loop-back[a]	25.9	$<$4.5

[a]Total loss is end-to-end (see IN!OUT in Fig. 10), thus including two times all losses, except for the InP on-chip loss, which is in there only once.

measurements of this experiment, since that would have caused large differences in the measured power of adjacent positions, and those have not been observed. When overdriving the position in the *z*-direction, the fingers eventually jump out of the funnel and land somewhere on the surface of the PIC. After such events in separate measurements, we have not seen changes in measured power or observed significant damage after SEM inspection of the funnel end.

As described before the *y* and *z* positions are correlated: due to the initial angle at which the fingers hit the surface of the chip, a lowering of the finger-holder will cause a shift of the finger tip in the positive *z*-direction. The effect of this can be seen in Figs. 11 and 12: the maximum power level for each *y* position varies by less than 0.4 dB for the whole 4 μm movement range. This placement tolerance is well within the accuracy and repeatability provided by current commercial automated wafer probe systems which demonstrates the potential for this optical probe to be integrated in such systems [25], [26], enabling simultaneous electrical and optical probing.

3.3 Analysis of the Coupling Efficiency

To evaluate the absolute coupling performance of the probe, we analyze the experimental data obtained with the procedure described in the previous Section 3.2. The output optical power of the broadband source OLS15CL was set at 12 dBm, resulting in 9.0 dBm after the 50/50 coupler. The power transmission results shown in Fig. 11 were normalized to the maximum -16.7 dBm optical power measured in the power meter. This means that we have a total link loss of 25.9 dB from the output of the coupler to the power meter. To understand this result, a more in-depth analysis is required and the loss mechanisms in each interface and in each optical path need to be evaluated.

The interfaces are identified and described in Fig. 13 and in Table 1. We present a detailed estimation of the optical loss in each interface and each optical path as well as the expected losses that should be achievable in an optimized next generation of the optical probe.

Fiber to probe—The first interface is the connection between the fiber array unit and the TriPleX probe chip. The optical loss in the fiber to probe coupling is estimated to be 1.5 dB due to tolerances in the multiprobe assembly and the mode mismatch between the InP and multiprobe.

Probe chip—On the probe chip, both the mode size and the waveguide pitch is adapted from fiber-matched to waveguide pitch (either 25 or 50 μm). We estimate 0.5 dB of propagation losses in the oxynitride chip. In an optimized device, we estimate the the losses can be reduced to 0.5 dB (fiber to probe) and 0.2 dB (on-chip propagation), by better control of the alignment and fixation processes between the FAU and the probe and by reducing the optical path length.

Probe to InP chip—The coupling interface between the probe and the InP chip includes a number of minimizable components. First we need to account for the Fresnel reflection losses caused by the change of refractive index. This results in 0.2 dB for the interface between the finger facet and air and in 1.9 dB for the interface between air and InP. Both contributions can be effectively eliminated by using anti-reflection (AR) coatings, which have not been applied to the current devices. Secondly, we analyzed the loss contribution from the mode size mismatch between the probe waveguide and the InP waveguide, which we estimate to be 1.7 dB, by calculating the overlap of the fundamental modes of both waveguides with dimensions as obtained from the fabricated samples, which differed from their design values. We expect that the mode mismatch can be reduced to below 0.3 dB by optimising the design and fabrication of the probe waveguides. The losses associated with the z-distance (longitudinal) due to diffraction are estimated to be 3.0 dB in the current design, based on 3D FDTD simulations [27]. This originates from the minimum distance between the probe and the InP PIC, which is 2.5 μm in our current design, corresponding to the distance d defined in the design of the InP funnel (see Fig. 3). This distance can be minimized in a next generation. By reducing the distance to below 1 μm, which fits well within fabrication capabilities, the loss can be reduced to below 0.5 dB, according to FDTD simulations [27].

In this generation of optical probes we faced a problem in controlling the thickness of the top cladding of the flexible waveguides which resulted in a misalignment between the two waveguide cores of 600 nm in the vertical direction. This had a major impact in the coupling, adding an extra 3.5 dB per coupling. For the next fabrication, the top cladding should be within the specified value and the impact on the loss should be kept below 0.2 dB for a 200 nm maximum misalignment between the two platforms.

InP chip—Finally, we account for 1.3 dB for the propagation losses in the InP chip, for approximately 5 mm waveguide at 2.5 dB/cm transmission loss for this device [1].

Thus, the total measured loss (25.9 dB) are now accounted for and two times 10.7 dB is attributed to the probe-to-chip interface. In addition, realistic values for an optimized probe have been justified which, in the same loop-back configuration, could realistically achieve less than 4.5 dB total loss for an optical path from source to detector. For a single coupling, the expected interface loss between the probe tip and the InP is thus expected to be $<$0.9 dB. This suggests that the application of the multiprobe can be extended to act as an interposer providing a permanent optical connection for packaging of PICs.

3.4 On-Wafer Spectral Measurements

We demonstrate the on-wafer measurement capabilities that are enabled by the optical probe with an example of measuring the modal gain spectrum of on-chip semiconductor optical amplifiers (SOAs). Fig. 14 shows the optical probe on the sample and the probe needles that apply the current to the amplifiers. We use the variable strip-length method described in [28], [29]. This method uses a multi-section SOA and different injection currents applied to different combinations of SOA length sections. For each current and SOA length setting it measures the generated optical amplified stimulated emission (ASE) spectrum with an optical spectrum analyzer. For this method to yield accurate results, it is important that the coupling efficiency to the output of multi-section SOA does not change during the measurements and that no extra reflections are added by the probe. One cause for the variation of the coupling efficiency is the thermal variation of the InP chip. Since the current to the SOA sections is varied, the temperature of the chip will change

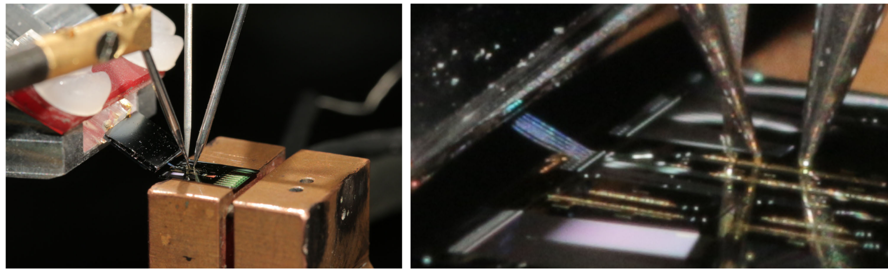

Fig. 14. (left) View of fingers landed on sample for performing the SOA gain measurements. (right) Zoomed-in view showing the fingers at the probe tip.

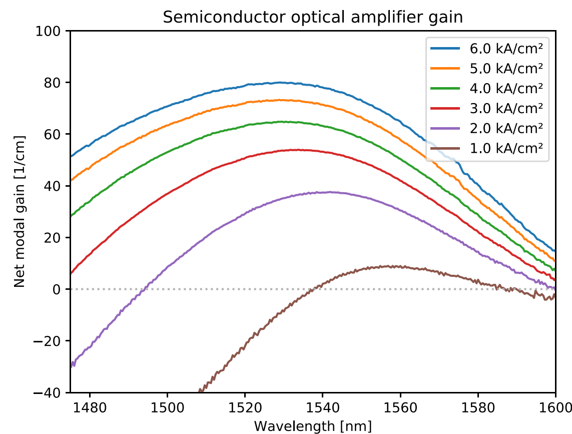

Fig. 15. Measured SOA gain.

and therefore also the position of the output waveguide. The typical measurement method, which uses a single lensed fiber to couple light out of the chip, requires active alignment after each change of the current setting [29]. Here, because of the flexibility of the optical probe and the tolerance to position changes, the measurements with the optical probe are not affected by these movements. The extracted modal gain versus wavelength for different current densities is shown in Fig. 15. The results are in agreement to those reported with the measurements that use a lensed fiber [29] with the advantage that the alignment was passive and no re-alignment is needed during the measurement. In addition, these gain test structures can be placed in any location on the PIC or the wafer and the measurement can be performed before cleaving the wafer into individual samples. This makes the probe also an enabler for on-chip measurements of process control modules [30].

4. Summary and Conclusions

In this paper we have described a new high-density multiport optical probe that enables large scale testing of photonic integrated circuits. The device is fabricated in an oxynitride photonics platform where, by locally removing the substrate, flexible waveguides beams are formed. In this work we have fabricated and tested probes with 4, 8 and 32 optical ports with two different pitches of 25 and 50 μm showing the density and scalability of the solution to a high number of ports. The pitch between the flexible waveguides could be reduced to below the demonstrated value of 25 μm, if needed. We believe that a 10 μm pitch would be feasible, when reducing both the width of the fingers and the gap between them.

We have shown coupling from a 32-channel optical probe to an InP PIC and described its calibration. The alignment between the probe and a PIC is passive and has proven to be fast

and accurate. The placement requirement tolerance was determined to be more than 4 μm in all directions, for less than 0.5 dB excess coupling loss. Because of this tolerance, a thermal expansion-mismatch between probe and circuit will not deteriorate the coupling efficiency and the large tolerance allows low-loss and reproducible coupling with existing wafer-probe accuracy. The measured loss of the probe coupling was high due to a non-optimized fabrication process. With realistic assumptions we have shown that the fiber-to-chip coupling loss can be expected to be less than 1.6 dB, while maintaining the excellent alignment tolerances.

An experimental demonstration of the combination of optical multi-probe measurements and electrical measurements was performed. For this, an on-chip measurement of the small-signal gain of SOAs was performed. The experimental results showed the potential of this approach for absolute wavelength measurement and demonstrates the stability of the coupling during the measurement. The results also show that the measurement accuracy is not affected by the thermal movement of the InP sample. The alignment tolerances in combination with the compatibility with electrical measurements prove the potential of implementing this solution in standard wafer probe testing systems.

All the experimental tests of the optical probes were performed on two different InP photonic integration platforms. Similar probes would be compatible with other edge-emitting photonic technologies. Finally, we have shown that the same device concept can be extended as an interposer to provide permanent connections for packaging of photonic ICs with much relaxed alignment demands and offering the option to connect many tens of optical fibers with a demonstrated density up to 40 connections per mm.

Acknowledgment

We thank Lionix international for fabrication of the probe and Oclaro and SMART Photonics for the fabrication of the InP PICs. The authors also acknowledge Sylwester Latkowski from Eindhoven University of Technology for valuable discussions and comments and Florian Lemaître from Eindhoven University of Technology for the photographs shown in Fig. 14.

References

[1] M. Smit, J. van der Tol, and M. Hill, “Moore’s law in photonics,” *Laser Photon. Rev.*, vol. 6, no. 1, pp. 1–13, 2012. [Online]. Available: https://dx.doi.org/10.1002/lpor.201100001

[2] H. Liu, C. F. Lam, and C. Johnson, “Scaling optical interconnects in datacenter networks opportunities and challenges for WDM,” in *Proc. 18th IEEE Symp. High Perform. Interconnects*, 2010, pp. 113–116.

[3] G. Roelkens *et al.*, “Silicon-based photonic integration beyond the telecommunication wavelength range,” *IEEE J. Sel. Topics Quantum Electron.*, vol. 20, no. 4, pp. 394–404, Aug. 2014.

[4] C. Kopp *et al.*, “Silicon photonic circuits: On-CMOS integration, fiber optical coupling, and packaging,” *IEEE J. Sel. Topics Quantum Electron.*, vol. 17, no. 3, pp. 498–509, May/Jun. 2011.

[5] P. Liao *et al.*, “Ultradense silicon photonic interface for optical interconnection,” *IEEE Photon. Technol. Lett.*, vol. 27, no. 7, pp. 725–728, Apr. 2015.

[6] T. Barwicz *et al.*, “A novel approach to photonic packaging leveraging existing high-throughput microelectronic facilities,” *IEEE J. Sel. Topics Quantum Electron.*, vol. 22, no. 6, pp. 455–466, Nov.-Dec. 2016.

[7] R. A. Boudreau and S. M. Boudreau, *Passive Micro-Optical Alignment Methods.* Boca Raton: Taylor & Francis, 2005, ISBN 9781315220994.

[8] G. Böttger, H. Schröder, and R. Jordan, “Active or passive fiber-chip-alignment: Approaches to efficient solutions,” *in Optoelectronic Interconnects XIII, A. L. Glebov and R. T. Chen, Eds.*, vol. 8630, Int. Soc. Opt. Photonics. SPIE, 2013, pp. 33–49. [Online]. Available: https://doi.org/10.1117/12.2014176

[9] D. Taillaert, P. Bienstman, and R. Baets, “Compact efficient broadband grating coupler for silicon-on-insulator waveguides,” *Opt. Lett.*, vol. 29, no. 23, pp. 2749–2751, Dec. 2004. [Online]. Available: https://ol.osa.org/abstract.cfm?URI=ol-29-23-2749

[10] D. Taillaert *et al.*, “Grating couplers for coupling between optical fibers and nanophotonic waveguides,” *Jpn. J. Appl. Phys.*, vol. 45, no. 8a, pp. 6071–6077, 2006.

[11] T. Miura, Y. Maeda, S. Matsuo, and H. Fukuda, “Wafer-level inspection platform on high-volume photonic integrated circuits for drastic reduction of testing time,” *in Optical Measurement Systems Industrial Inspection XI, P. Lehmann, W. Osten, and A. A. G. Jr., Eds.*, vol. 11056, International Society for Optics and Photonics. SPIE, 2019, pp. 698–704. [Online]. Available: https://doi.org/10.1117/12.2527382

[12] H. D. Thacker, O. O. Ogunsola, A. V. Mule, and J. D. Meindl, “Wafer-testing of optoelectonic-gigascale CMOS integrated circuits,” *IEEE J. Sel. Topics Quantum Electron.*, vol. 17, no. 3, pp. 659–670, May/Jun. 2011.
[13] S. Jordan, Practical Examples of Parallel Alignment Automation (White Paper). Physik Instrumente (PI) GmbH & Co, 2018. [Online]. Available: https://static.physikinstrumente.com/fileadmin/user_upload/physik_instrumente/files/WP/PI-WP4010E-Practical-Examples-of-Parallel-Alignment-Automation.pdf, Accessed 5 October 2020.
[14] J. De Coster *et al.*, “Test-station for flexible semi-automatic wafer-level silicon photonics testing,” in *Proc. 21th IEEE Euro. Test Symp.*, May 2016, pp. 1–6.
[15] T. Gnausch, A. Grundmann, T. Juhasz, T. Kaden, R. Böttner, and T. von Freyhold, “Novel opto-electronical probe card for wafer-level PIC testing,” in *Proc. Opt. Fiber Commun. Conf. Opt. Soc. Amer.*, 2019, p. Th2A.1. [Online]. Available: https://www.osapublishing.org/abstract.cfm?URI=OFC-2019-Th2A.1
[16] R. Polster, L. Y. Dai, O. A. Jimenez, Q. Cheng, M. Lipson, and K. Bergman, “Wafer-scale high-density edge coupling for high throughput testing of silicon photonics,” in *Proc. Opt. Fiber Commun. Conf. Opt. Soc. Amer.*, 2018, p. M3F.2. [Online]. Available: https://www.osapublishing.org/abstract.cfm?URI=OFC-2018-M3F.2
[17] M. Trappen *et al.*, “3D-printed optics for wafer-scale probing,” in *Proc. 44th Eur. Conf. Opt. Comm.*, 2018, pp. 1–3.
[18] E. Bitincka, “Generic testing in photonic ICs,” Ph.D. dissertation, Eindhoven Univ. Technol., Eindhoven, Dept. Elect. Eng., The Netherlands, 2015, ISBN 978-94-6295-091-7.
[19] P. Vettiger *et al.*, “Full-wafer technology-a new approach to large-scale laser fabrication and integration,” *IEEE J. Quantum Electron.*, vol. 27, no. 6, pp. 1319–1331, Jun. 1991.
[20] R. Santos, D. D’Agostino, F. Soares, H. Rabbani Haghighi, K. Williams, and X. Leijtens, “Fabrication of etched facets and vertical couplers in InP for packaging and on-wafer test,” *IEEE Photon. Technol. Lett.*, vol. 28, no. 3, pp. 245–247, Feb. 2016.
[21] K. Wörhoff, R. G. Heideman, A. Leinse, and M. Hoekman, “TriPleX: A versatile dielectric photonic platform,” *Adv. Opt. Techn.*, vol. 4, no. 2, pp. 189–207, 2015.
[22] M. Smit *et al.*, “An introduction to InP-based generic integration technology,” *Semicond. Sci. Technol.*, vol. 29, no. 8, 2014. Art. no. 083001.
[23] L. M. Augustin *et al.*, “InP-Based generic foundry platform for photonic integrated circuits,” *IEEE J. Sel. Topics Quantum Electron.*, vol. 24, no. 1, pp. 1–10, Jan. 2018.
[24] E. E. Friedrich, M. G. Öberg, B. Broberg, S. Nilsson, and S. Valette, “Hybrid integration of semiconductor lasers with si-based single-mode ridge waveguides,” *J. Lightw. Technol.*, vol. 10, no. 3, pp. 336–339, Mar. 1992.
[25] “MPI corporation, Taiwan,” Accessed: Mar. 1, 2020. [Online]. Available: https://www.mpi-corporation.com/wp-content/uploads/ASTPDF/MPI-TS2000-SE-Automated-Probe-System-Data-Sheet.pdf
[26] “Accretech Tokyo Seimitsu: UF2000,” Accessed: Mar. 1, 2020. [Online]. Available: https://www.accretech.eu/en/products/semiconductor/wafer-probing-machines/uf2000/
[27] Lumerical, Inc. 3D FDTD: 3D Electromagnetic Simulator. [Online]. Available: https://www.lumerical.com/products/.
[28] J. Thomson, H. Summers, P. Hulyer, P. Smowton, and P. Blood, “Determination of single-pass optical gain and internal loss using a multisection device,” *Appl. Phys. Lett.*, vol. 75, no. 17, pp. 2527–2529, Oct. 1999.
[29] D. Pustakhod, K. Williams, and X. Leijtens, “Fast and robust method for measuring semiconductor optical amplifier gain,” *IEEE J. Sel. Topics Quantum Electron.*, vol. 24, no. 1, pp. 1–9, Jan. 2018.
[30] D. Pustakhod, “Process control modules for photonic integration technology,” Ph.D. dissertation, Technische Universiteit Eindhoven, Eindhoven, Dept. Elect. Eng., The Netherlands, 2018, ISBN 978-90-386-4529-2.